Published in IET Power Electronics
Received on 31st January 2010
Revised on 14th July 2010
doi: 10.1049/iet-pel.2010.0040

ISSN 1755-4535

Transformer winding loss caused by skin and proximity effects including harmonics in pulse-width modulated DC–DC flyback converters for the continuous conduction mode

D. Murthy-Bellur[1] *N. Kondrath*[2] *M.K. Kazimierczuk*[3]

[1]*School of Engineering, Pennsylvania State University, The Behrend College, Erie, PA 16563, USA*
[2]*Department of Electrical and Computer Engineering, University of Minnesota Duluth, Duluth, MN 55812, USA*
[3]*Department of Electrical Engineering, Wright State University, Dayton, OH 45435, USA*
E-mail: murthybellur.2@wright.edu

Abstract: High-frequency (HF) transformers used in pulse-width-modulated power converters conduct periodic non-sinusoidal HF currents, which give rise to additional winding losses caused by harmonics. This study presents expressions for winding power losses in a two-winding transformer with periodic non-sinusoidal primary and secondary current waveforms for flyback converters operating in the continuous conduction mode (CCM). Dowell's equation, which takes into account both the skin and proximity effects, is used to determine the primary and secondary winding resistances as functions of frequency. Fourier series of the primary and secondary current waveforms and the winding resistances are used to determine the winding power losses at harmonic frequencies. The harmonic primary and secondary winding loss factors F_{Rph} and F_{Rsh} are introduced for CCM operation. The theory is illustrated by performance evaluation of the transformer in a flyback converter in CCM over the entire range of converter operation. Power losses in the primary and secondary transformer windings are illustrated as functions of the output power and the DC input voltage.

1 Introduction

High-frequency (HF) transformers are an integral part of pulse-width-modulated (PWM) converters, which are widely used in many applications such as power-factor correctors, DC–DC power converters and electromagnetic interference (EMI) filters [1–5]. For low-power applications, flyback PWM DC–DC converter is a popular choice because of its low parts count when compared with other isolated DC–DC converter topologies. The HF transformer in a flyback converter is used to provide galvanic isolation and also to store the magnetic energy required for power conversion. Operating the flyback converter at high switching frequency reduces the size of the transformer, but increases the transformer winding losses caused by skin and proximity effects. Additionally, since transformers in isolated PWM converters conduct periodic non-sinusoidal currents in steady state, the spectra of the primary and secondary current waveforms of the transformer are very rich and the losses caused by the harmonics further increase the winding power losses. The harmonic losses in transformer windings at HF also increase the operating temperature.

HF effects in windings and cores were studied in several papers [6–29]. The winding AC resistance caused by the skin and proximity effects for sinusoidal current in a winding was presented in [6–8]. The theoretical analyses presented in [6–8] were further extended in [9–15]. In another method [16], the AC resistances for a number of arbitrary waveforms were determined using the rms values of the current waveforms and the rms values of its derivatives. Methods to design inductors and transformers for PWM converters are available in [30–32]. However, the transformer design in [30] and other publications do not account for winding losses caused neither by HF skin and proximity effects nor by harmonics. Until now, the Fourier expansion of the flyback transformer primary and secondary current waveforms in PWM converters operating in the continuous conduction mode (CCM) as shown in Fig. 1 has not been presented in the literature.

The objectives of this paper are (i) to develop winding power loss equations for a two-winding transformer conducting periodic non-sinusoidal HF currents containing DC components and harmonics such as those in flyback PWM converters [33–35] operating in CCM, using Dowell's theory and the methods developed in [36–38], (ii) to give a step-by-step procedure to design a two-winding transformer for flyback converter operated in CCM, using the area product method and (iii) to study the effect of harmonics on winding losses in the transformer of a flyback PWM DC–DC converter in CCM over the entire range of converter operation.

Sections 2 and 3 present the derivations of core area product and winding power loss equations for a flyback transformer in CCM conducting periodic non-sinusoidal

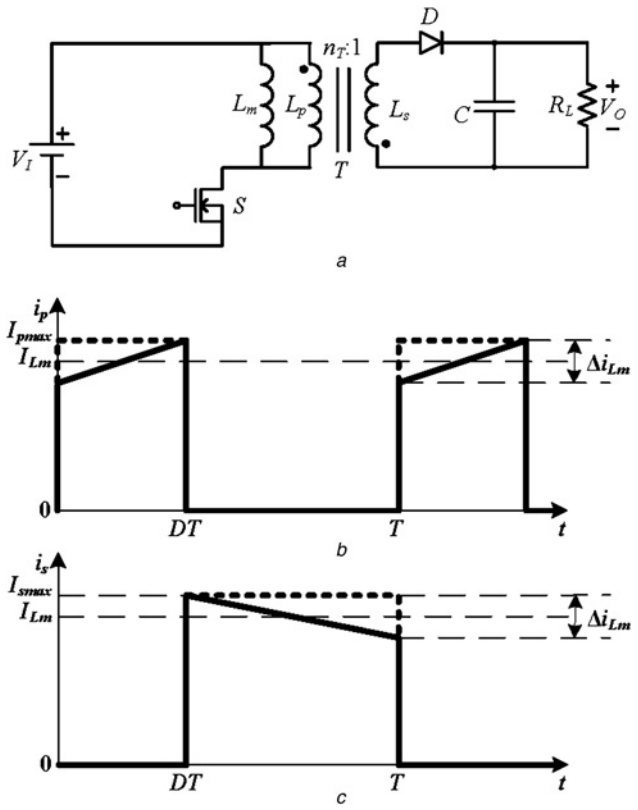

Fig. 1 *Flyback converter circuit and two-winding flyback transformer current waveforms for CCM operation*

a Flyback PWM DC–DC converter circuit
b Primary winding current i_p
c Secondary winding current i_s

current waveforms, respectively. The procedure to design a two-winding transformer for a flyback PWM DC–DC converter operated in CCM is given in Section 4. In Section 5, the performance evaluation of the designed flyback transformer is given. Experimental and simulation results are presented in Section 6. Finally, conclusions and discussions are given in Section 7.

2 Core area product for a two-winding flyback transformer

The instantaneous magnetic flux linkage of the primary winding is given by

$$\lambda(t) = N_p \phi(t) = N_p A_c B(t) = L_p i_p(t) \tag{1}$$

where $\phi(t)$ is the instantaneous magnetic flux linking N_p turns of the primary winding of the transformer, A_c is the core cross-sectional area in m^2, L_p is the inductance of the primary winding, $i_p(t)$ is the instantaneous current in the primary winding and $B(t)$ is the instantaneous magnetic flux density in T. Equation (1) for the peak values becomes

$$\lambda_{pk} = N_p \phi_{pk} = N_p A_c B_{pk} = L_p I_{p\max} \tag{2}$$

The maximum current density of the primary winding wire is

$$J_m = \frac{I_{p\max}}{A_{wp}} \tag{3}$$

where A_{wp} is the bare wire cross-sectional area of the primary winding in m^2. The window area limited by the maximum current density in both primary and secondary windings is given by

$$W_a = \frac{N_p A_{wp} + N_s A_{ws}}{K_u} \tag{4}$$

where N_s is the number of turns in the secondary winding, A_{ws} is the secondary winding bare wire cross-sectional area in m^2 and K_u is the window utilisation factor. Assuming the winding allocation is such that $N_p A_{wp} = N_s A_{ws}$, the window area is

$$W_a = \frac{2N_p A_{wp}}{K_u} \tag{5}$$

where the window utilisation factor is defined as

$$K_u = \frac{A_{Cu}}{W_a} = \frac{2N_p A_{wp}}{W_a} \tag{6}$$

where A_{Cu} is the total copper cross-sectional area in the window in m^2. The maximum energy stored in the magnetic field of the transformer is $W_m = (1/2)L_m I^2_{Lm\max}$, where L_m is the magnetising inductance on the primary side and I_{Lm} is the current through the magnetising inductance L_m. Assuming that $L_p \simeq L_m$ and $I_{pmax} \simeq I_{Lm(max)}$, and using (2), (3) and (5), the area product of the core is defined as

$$A_p = W_a A_c = \frac{2L_p I^2_{p\max}}{K_u J_m B_{pk}} = \frac{4W_m}{K_u J_m B_{pk}} \tag{7}$$

In (7), $B_{pk} < B_s$, where B_s is the core saturation flux density at the highest operating temperature. The area product A_p is a measure of energy handling capability of a core and can be used to select a suitable core using the manufacturer's datasheets.

3 Copper power loss for flyback transformer conducting periodic non-sinusoidal current in CCM

In transformers used in isolated PWM DC–DC power converters in CCM, the current waveforms through the primary and secondary windings are pulsating. Therefore the amplitudes of the harmonics are high, resulting in high winding losses. This situation is different in non-isolated PWM converters in CCM because the current waveform of the inductor is nearly constant and the amplitudes of harmonics are low as compared to the DC component [38].

3.1 Primary winding power loss

Assume that the primary winding current for CCM is a rectangular waveform with a duty ratio D as shown in Fig. 1*b*. The primary winding current waveform is given by

$$i_p \simeq \begin{cases} I_{p\max}, & \text{for } 0 < t \le DT \\ 0, & \text{for } DT < t \le T \end{cases} \tag{8}$$

doi: 10.1049/iet-pel.2010.0040

The DC component of the primary winding current waveform for CCM is

$$I_{\mathrm{pdc}} = \frac{1}{T}\int_0^T i_{\mathrm{p}}\mathrm{d}t = \frac{I_{\mathrm{p\,max}}}{T}\int_0^{DT}\mathrm{d}t = DI_{\mathrm{p\,max}} \tag{9}$$

The Fourier series of the current waveform in the primary winding is

$$i_{\mathrm{p}} = I_{\mathrm{pdc}}\left[1 + 2\sum_{n=1}^{\infty}\frac{\sin(n\pi D)}{n\pi D}\cos(n\omega_{\mathrm{s}}t)\right] \tag{10}$$

and the amplitudes of the fundamental component and the harmonics of the primary current waveform for CCM is

$$I_{\mathrm{p}n} = \frac{2I_{\mathrm{p\,max}}}{n\pi}\sin(n\pi D) = \frac{2I_{\mathrm{pdc}}}{n\pi D}\sin(n\pi D) \tag{11}$$

The AC resistance factor F_R obtained from Dowell's one-dimensional solution in Cartesian coordinates [7] is

$$F_R = \frac{R_{\mathrm{w}}}{R_{\mathrm{wdc}}} = F_{\mathrm{s}} + F_{\mathrm{p}} = A\left[\frac{\sinh(2A)+\sin(2A)}{\cosh(2A)-\cos(2A)} + \frac{2(N_l^2-1)}{3}\frac{\sinh(A)-\sin(A)}{\cosh(A)+\cos(A)}\right] \tag{12}$$

where the first term represents the skin effect winding AC resistance factor F_{S} and the second term describes the proximity effect winding AC resistance factor F_{P}. The power loss in the primary winding for CCM is

$$\begin{aligned} P_{\mathrm{wp}} &= R_{\mathrm{wpdc}}I_{\mathrm{pdc}}^2\left[1 + \frac{1}{2}\sum_{n=1}^{\infty}\left(\frac{R_{\mathrm{wp}n}}{R_{\mathrm{wpdc}}}\right)\left(\frac{I_{\mathrm{p}n}}{I_{\mathrm{pdc}}}\right)^2\right] \\ &= P_{\mathrm{wpdc}}\left[1 + \frac{1}{2}\sum_{n=1}^{\infty}F_{R\mathrm{p}n}\left(\frac{I_{\mathrm{p}n}}{I_{\mathrm{pdc}}}\right)^2\right] \\ &= P_{\mathrm{wpdc}}\left\{1 + 2\sum_{n=1}^{\infty}F_{R\mathrm{p}n}\left[\frac{\sin(n\pi D)}{n\pi D}\right]^2\right\} \\ &= P_{\mathrm{wpdc}}R_{\mathrm{wp}n} \end{aligned} \tag{13}$$

where the normalised primary winding resistance at the fundamental frequency and harmonic frequencies obtained from (12) is

$$F_{R\mathrm{p}n} = \frac{R_{\mathrm{wpn}}}{R_{\mathrm{wpdc}}} = F_{\mathrm{S}n} + F_{\mathrm{P}n} = A\sqrt{n} \times \left[\frac{\sin(2A\sqrt{n})+\sin(2A\sqrt{n})}{\cosh(2A\sqrt{n})-\cos(2A_{\mathrm{p}}\sqrt{n})} + \frac{2(N_l^2-1)}{3}\frac{\sinh(A\sqrt{n})-\sin(A\sqrt{n})}{\cosh(A\sqrt{n})+\cos(A\sqrt{n})}\right] \tag{14}$$

The factor $F_{\mathrm{Rp}n}$ takes into account the skin and proximity effects in the winding. Note that F_R and $F_{\mathrm{Rp}n}$ are different as the latter is dependent on the nth harmonic of the primary winding current waveform. The primary winding harmonic loss factor is defined as the total primary winding loss consisting of DC and AC power losses normalised with respect to the primary winding DC power loss given by

$$F_{\mathrm{Rph}} = \frac{P_{\mathrm{wp}}}{P_{\mathrm{wpdc}}} = 1 + 2\sum_{n=1}^{\infty}F_{R\mathrm{p}n}\left[\frac{\sin(n\pi D)}{n\pi D}\right]^2 \tag{15}$$

The skin depth of the winding conductor at the nth harmonic is

$$\delta_{\mathrm{w}n} = \frac{\delta_{\mathrm{w1}}}{\sqrt{n}} \tag{16}$$

where $\delta_{\mathrm{w1}} = \sqrt{\rho/\pi\mu_0 f}$ is the conductor skin depth at the fundamental frequency f, which is equal to the converter switching frequency f_{s}. The winding conductor thickness normalised with respect to the conductor skin depth is

$$A_n = \frac{h}{\delta_{\mathrm{w}n}} = \frac{h\sqrt{n}}{\delta_{\mathrm{w1}}} = A\sqrt{n} \tag{17}$$

where the normalised winding conductor thickness at the fundamental frequency for a rectangular conductor is [39]

$$A = \frac{h}{\delta_{w1}}\sqrt{\frac{w}{p}} \tag{18}$$

for a square conductor is [39]

$$A = \frac{h}{\delta_{w1}}\sqrt{\frac{h}{p}} \tag{19}$$

and for a round conductor is [39]

$$A = \left(\frac{\pi}{4}\right)^{3/4}\frac{d}{\delta_{w1}}\sqrt{\frac{d}{p}} \tag{20}$$

In (18), (19) and (20), w/p, h/p and d/p are called the layer porosity factors, w is the width of the rectangular bare conductor, h is the thickness of the square and rectangular bare conductors, d is the diameter of the round bare conductor and p is the distance between the centres of two adjacent conductors, called the winding pitch.

3.2 Secondary winding power loss

Assume that the secondary winding current for CCM is a rectangular waveform as shown in Fig. 1*c*. The secondary winding current is given by

$$i_{\mathrm{s}} \simeq \begin{cases} 0, & \text{for } 0 < t \le DT \\ I_{\mathrm{s\,max}}, & \text{for } DT < t \le T \end{cases} \tag{21}$$

The DC component of the secondary winding current waveform for CCM is

$$I_{\mathrm{sdc}} = \frac{1}{T}\int_0^T i_{\mathrm{s}}\mathrm{d}t = \frac{I_{\mathrm{s\,max}}}{T}\int_{DT}^T\mathrm{d}t = (1-D)I_{\mathrm{s\,max}} \tag{22}$$

Table 1 Two-winding transformer design for flyback PWM DC–DC converter in CCM

Step number	Parameter	Equation	Value
	Converter specifications		
1	input voltage	V_I	50 ± 10 V
2	output voltage	V_O	24 V
3	switching frequency	f_s	100 kHz
4	output power	$P_{O\max}(P_{O\min})$	30 W (5 W)
	Design equations for the transformer in flyback converter		
5	maximum load resistance	$R_{L\max} = \frac{V_O^2}{P_{O\min}}$	115.2 Ω
6	minimum DC voltage transfer function	$M_{VDC\min} = \frac{V_O}{V_{I\max}}$	0.4
7	maximum DC voltage transfer function	$M_{VDC\max} = \frac{V_o}{V_{I\min}}$	0.6
8	transformer primary-to-secondary turns ratio*	$n_T = \frac{n_{conv} D_{\max}}{(1 - D_{\max}) M_{VDC\max}}$	1.5
9	minimum duty cycle	$D_{\min} = \frac{n_T M_{VDC\min}}{n_T M_{VDC\min} + n_{conv}}$	0.4
10	minimum magnetising inductance for CCM	$L_p \simeq L_{m(\min)} = \frac{n_T^2 R_{L\max}(1 - D_{\min})^2}{2 f_1}$	466 μH pick 500 μH
11	secondary winding inductance	$L_s = \frac{L_p}{n_T^2}$	222 μH
12	maximum peak-to-peak primary winding current	$\Delta i_{Lp(\max)} = \Delta i_{Lm(\max)} = \frac{n_T V_o (1 - D_{\min})}{f_s L_p}$	0.43 A
13	maximum DC input current	$I_{I\max} = \frac{M_{VDC\max} I_{O\max}}{\eta_{conv}}$	0.83 A
14	maximum peak primary winding current	$I_{p\max} = \frac{I_{O\max}}{n_T(1 - D_{\max})} + \frac{n_T V_O (1 - D_{\max})}{2 f_s L_D}$	1.84 A
	Area product		
15	window utilisation factor	K_u	0.3
16	peak flux density	B_{pk}	0.31 T
17	maximum current density of the winding wire	J_m	6 A/mm^2
18	maximum energy stored in the transformer magnetic field	$W_m = \frac{1}{2} L_p I_{p\max}^2$	0.85 mJ
19	core area product (calculated)	$A_p = W_a A_c = \frac{4 W_m}{K_u J_m B_{pk}}$	0.61 cm^4
	Core selection		
20	selected core	magnetics ferrite *p*-type round-slab (RS) core	0P-43019
21	area product of the selected core	A_p	0.63 cm^4
22	core cross-sectional area	A_c	1.23 cm^2
23	core window area	W_a	0.51 cm^2
24	mean magnetic path length	l_c	4.56 cm
25	mean length of single turn	l_T	6.05 cm
26	core volume	V_c	5.61 cm^3
27	core permeability	μ_{rc}	2500 ± 25%
28	core saturation flux density	B_s	0.49 T
29	coefficients in core power loss density equation (for *p*-type ferrite material and 100 kHz ≤ f_s < 500 kHz)	$P_v = k(f_s \text{ in kHz})^a (10 B_m)^b$	
29(a)		k	0.0434
29(b)		a	1.63
29(c)		b	2.62
	Wire selection		
30	skin depth of copper wire (at 20°C and f_s = 100 kHz)	$\delta_{w1} = \sqrt{\frac{\rho_{cu}(20^\circ\text{C})}{\pi f_s \mu_0}}$	0.209 mm
31	selected copper wire	AWG	No. 26
32	bare wire diameter of the strand wire	d_{is}	0.40 mm
33	insulated wire diameter of the strand wire	d_{os}	0.45 mm
34	bare wire cross-sectional area of the strand	A_{wsi}	0.12 mm^2
35	insulated wire cross-sectional area of the strand	A_{wso}	0.16 mm^2
36	DC resistance of the strand per unit length	R_{wdc}/l_w	0.1345 Ω/m
	Primary winding design		
37	cross-sectional area of the primary winding wire	$A_{wp} = \frac{I_{p\max}}{J_m}$	0.30 mm^2

Continued

doi: 10.1049/iet-pel.2010.0040

Table 1 *Continued*

Step number	Parameter	Equation	Value
38	number of strands in the primary winding	$s_p = \frac{A_{wp}}{A_{wsi}}$	2.38 pick 2
39	number of turns of the primary winding	$N_p = \frac{K_u(W_a/2)}{S_p A_{wsi}}$	29.82 pick 30
40	total length of the primary winding wire	$l_{wp} = N_p l_T$	181.5 cm pick 187 cm
	Primary winding losses		
41	primary strand DC and low-frequency resistance	$R_{wpdcs} = \left(\frac{R_{wdc}}{l_w}\right) l_{wp}$	251.5 mΩ
42	primary winding wire DC and low-frequency resistance	$R_{wpdc} = \frac{R_{wpdcs}}{S_p}$	125.8 mΩ
43	primary winding DC and low-frequency power loss	$P_{wpdc} = R_{wpdc} I^2_{s\,max}$	0.087 W
44	primary winding harmonic loss factor	F_{Rph} (Use (15) @ V_{lmin}, P_{Omax})	5.195
45	primary winding total power loss	$P_{wp} = F_{Rph} P_{wpdc}$	0.453 W
	Secondary winding design		
46	maximum peak secondary winding current	$I_{s\,max} = n_T I_{p\,max}$	2.81 A
47	cross-sectional area of the secondary winding wire	$A_{ws} = \frac{I_{s\,max}}{J_m}$	0.46 mm^2
48	number of strands in the secondary winding	$S_s = \frac{A_{ws}}{A_{wsi}}$	3.63 pick 4
49	number of turns of the secondary winding	$N_s = \frac{N_p}{n_T}$	19.88 pick 20
50	total length of the secondary winding wire	$l_{ws} = N_s l_T$	121 cm pick 130 cm
	Secondary winding losses		
51	secondary strand DC and low-frequency resistance	$R_{wsdcs} = \left(\frac{R_{wdc}}{l_w}\right) l_{ws}$	0.174 Ω
52	secondary winding wire DC and low-frequency resistance	$R_{wsdc} = \frac{R_{wsdcs}}{S_s}$	43.71 mΩ
53	secondary winding DC and low-frequency power loss	$P_{wsdc} = R_{wsdc} I^2_{O\,max}$	0.068 W
54	secondary winding harmonic loss factor	F_{Rsh} (Use (26) @ V_{lmin}, P_{Omax})	5.19
55	secondary winding total power loss	$P_{ws} = F_{Rsh} P_{wsdc}$	0.354 W
	Total winding losses		
56	total DC and low-frequency power loss in both windings	$P_{wdc} = P_{wpdc} + P_{wsdc}$	0.155 W
57	total winding power loss	$P_w = P_{wp} + P_{ws}$	0.808 W
	Core losses		
58	air-gap length	$l_g = \frac{\mu_0 A_c N_p^2}{L_p} - \frac{l_c}{\mu_{rc}}$	0.26 mm
59	maximum peak magnetic flux density	$B_{pk} = \frac{\mu_0 N_p I_{p\,max}}{l_g + (l_c/\mu_{rc})}$	0.25 T
60	magnetic flux density AC component	$B_m = \frac{\mu_0 N_p}{l_g + (l_c/\mu_{rc})} \left(\frac{\Delta i_{Lp}}{2}\right)$	0.024 T
61	core power loss density	$P_v = k(f_s \text{ in kHz})^a (10 B_m)^b$	2.07 mW/cm^3
62	core loss	$P_c = V_c P_v$	10.99 mW
	Total losses, temperature rise and efficiency		
63	total transformer power loss	$P_{cw} = P_c P_w$	0.819 W
64	total core surface area	A_t	31.95 cm^2
65	surface power loss density	$\psi = \frac{P_{cw}}{A_t}$	0.025 W/cm^2
66	temperature rise of the transformer	$\Delta T = 450 \psi^{0.826}$	21.79°C
67	window utilisation factor (recalculated)	$K_u = \frac{(N_p s_p + N_s) A_{wsi}}{W_a}$	0.35
68	transformer efficiency at full power and V_{lmin}	$\eta_t = \frac{P_O}{P_O + P_{cw}}$	97.34%

*Assume converter efficiency $\eta = 0.9$ and $D_{max} = 0.5$

Table 2 List of symbols

A	winding conductor thickness normalised with respect to conductor skin depth
A_c	transformer core cross-sectional area in m^2
A_{Cu}	total wire cross-sectional area in the core window in m^2
A_p	area product in m^4
A_{wp}	bare wire cross-sectional area of the primary winding in m^2
A_{ws}	bare wire cross-sectional area of the secondary winding in m^2
B_{pk}	peak magnetic flux density in T
B_s	saturation magnetic flux density in T
D	converter duty cycle
F_R	winding AC resistance factor
F_{Rph}	primary winding harmonic loss factor
F_{Rsh}	secondary winding harmonic loss factor
I_{Lm}	magnetising inductance current in A
I_p	primary winding current in A
I_s	secondary winding current in A
J_m	winding wire maximum current density in A/m^2
K_u	window utilisation factor
L_m	magnetising inductance of the transformer in H
L_p	inductance of the primary winding in H
L_s	inductance of the secondary winding in H
N_p	number of turns of the primary winding of the transformer
N_s	number of turns of the secondary winding of the transformer
P_{wp}	primary winding power loss in W
P_{ws}	secondary winding power loss in W
T	time period of one switching cycle of the converter in s
W_a	core window area in m^2
W_m	maximum energy stored in the magnetic field of the transformer in J
δ_w	skin depth of the winding conductor in mm
λ	magnetic flux linkage in Wb-turns
φ	magnetic flux in Wb

The Fourier series of the current waveform in the secondary winding is

$$i_s = I_{sdc}\left[1 + 2\sum_{n=1}^{\infty}\frac{\sin[n\pi(1-D)]}{n\pi(1-D)}\cos(n\omega_s t)\right] \quad (23)$$

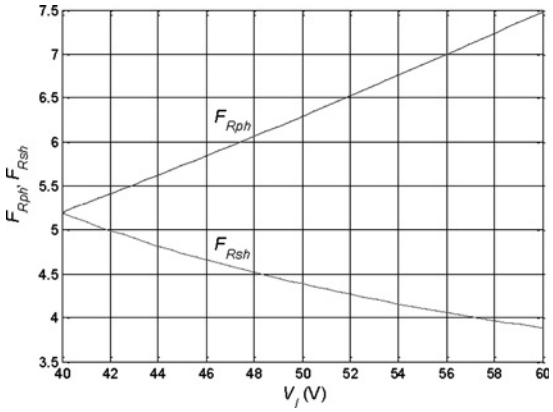

Fig. 2 *Primary winding harmonic loss factor F_{Rph} and secondary winding harmonic loss factor F_{Rsh} as functions of the DC input voltage V_I*

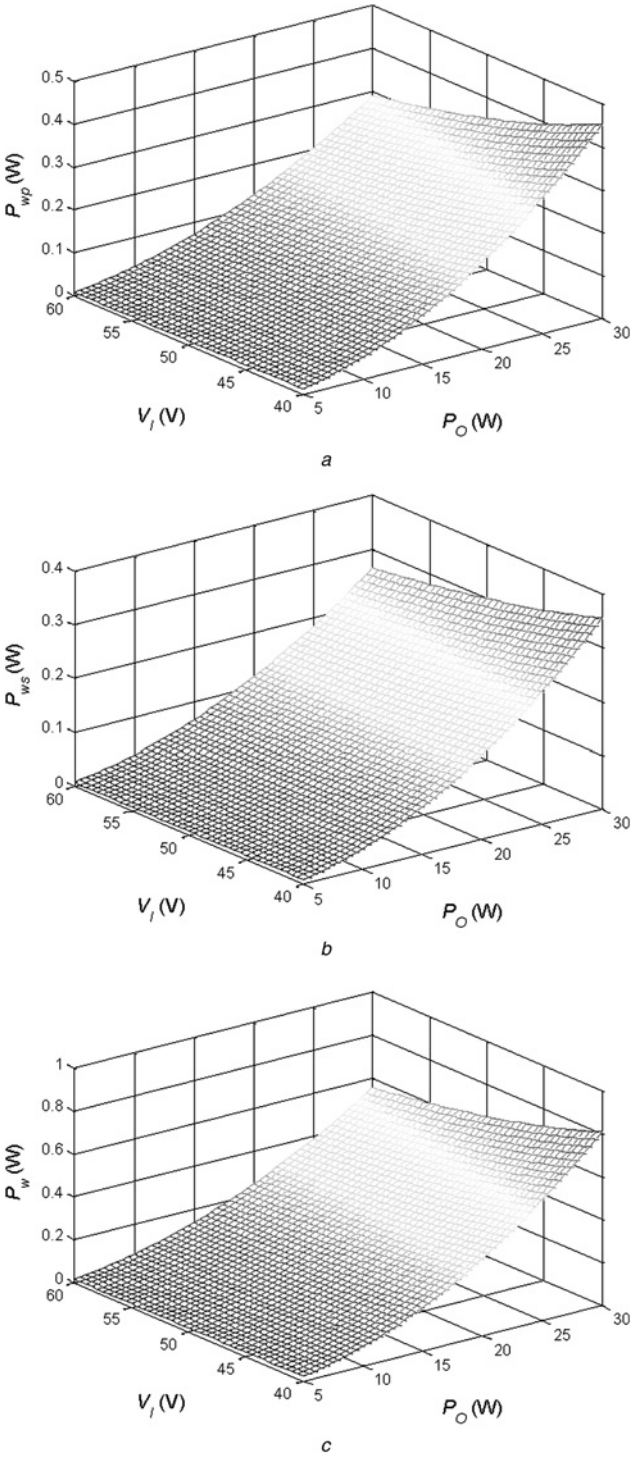

Fig. 3 *Winding power losses as functions of DC input voltage V_I and output power P_O*

a Primary winding loss P_{wp}
b Secondary winding loss P_{ws}
c Total winding loss P_w

and the amplitude of the fundamental component and the harmonics of the secondary winding current waveform for CCM is

$$I_{sn} = \frac{2I_{s\max}}{n\pi}\sin[n\pi(1-D)] = \frac{2I_{sdc}}{n\pi(1-D)}\sin[n\pi(1-D)] \quad (24)$$

doi: 10.1049/iet-pel.2010.0040

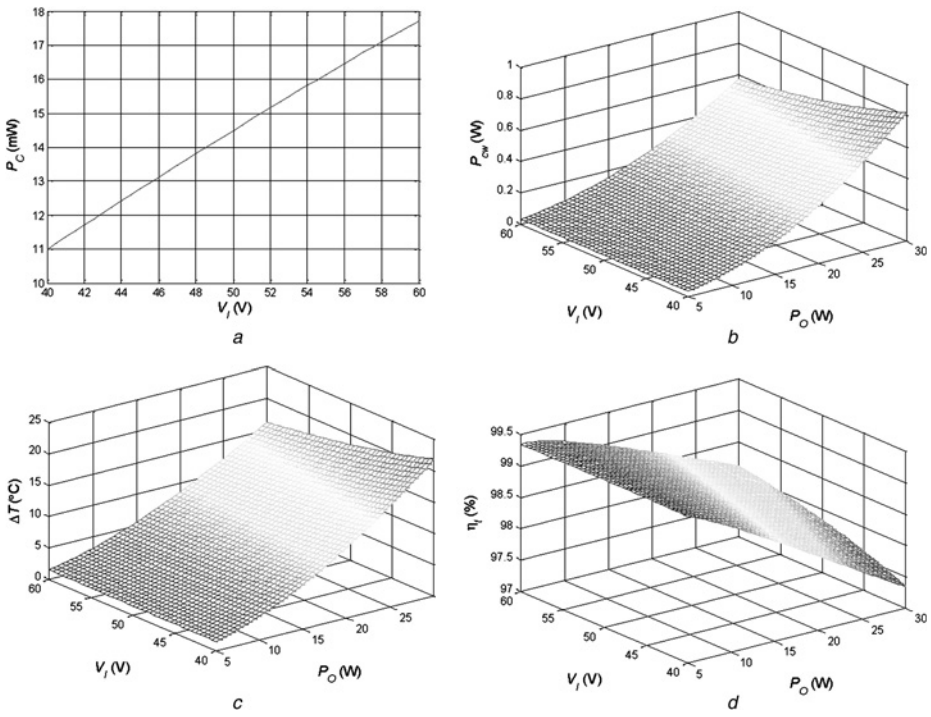

Fig. 4 *Core loss, total transformer loss, transformer temperature rise and transformer efficiency as functions of DC input voltage V_I and output power P_O*

a Core loss P_C
b Total transformer power loss P_{cw}
c Flyback transformer temperature rise ΔT
d Transformer efficiency η_t of the flyback converter in CCM

The power loss in the secondary winding for CCM is

$$\begin{aligned} P_{ws} &= R_{wsdc} I_{sdc}^2 \left[1 + \frac{1}{2} \sum_{n=1}^{2} \left(\frac{R_{wsn}}{R_{wsdc}} \right) \left(\frac{I_{sn}}{I_{sdc}} \right)^2 \right] \\ &= P_{wsdc} \left[1 + \frac{1}{2} \sum_{n=1}^{2} F_{Rsn} \left(\frac{I_{sn}}{I_{sdc}} \right)^2 \right] \\ &= P_{wsdc} \left\{ 1 + 2 \sum_{n=1}^{\infty} F_{Rsn} \left[\frac{\sin[n\pi(1-D)]}{n\pi(1-D)} \right]^2 \right\} \\ &= P_{wsdc} F_{Rsh} \end{aligned} \tag{25}$$

where the secondary winding DC power loss $P_{wsdc} = R_{wsdc} I_{sdc}^2$. The secondary winding harmonic loss factor is defined as the total secondary winding DC and AC power loss normalised with respect to the secondary winding DC power loss given by

$$F_{Rsh} = \frac{P_{ws}}{P_{wsdc}} = 1 + 2 \sum_{n=1}^{\infty} F_{Rsn} \left[\frac{\sin[n\pi(1-D)]}{n\pi(1-D)} \right]^2 \tag{26}$$

where

$$\begin{aligned} F_{Rsn} = \frac{R_{wsn}}{R_{wsdc}} &= F_{sn} + F_{pn} = A\sqrt{n} \\ &\times \left[\frac{\sinh(2A\sqrt{n}) + \sin(2A\sqrt{n})}{\cosh(2A\sqrt{n}) - \cos(2A_p\sqrt{n})} \right. \\ &\left. + \frac{2(N_l^2 - 1)}{3} \frac{\sinh(A\sqrt{n}) - \sin(A\sqrt{n})}{\cosh(A\sqrt{n}) + \cos(A\sqrt{n})} \right] \end{aligned} \tag{27}$$

In (26), F_{Rsn} can be computed using (27) for the secondary winding and using (18), (19) and (20) for rectangular, square or round secondary winding wire, respectively.

4 HF transformer design for a flyback converter in CCM

The above theory will be illustrated by the case study of the transformer used in the flyback converter operating in CCM. The following specifications of the flyback converter are used: DC input voltage $V_I = 50 \pm 10$ V, DC output voltage $V_O = 24$ V, maximum output power $P_{Omax} = 30$ W, minimum output power $P_{Omin} = 5$ W and switching frequency $f_s = 100$ kHz. Using the procedure for the flyback converter design [33], a step-by-step design procedure of the flyback transformer is given in Table 1. A list of symbols is given in Table 2. In Table 1, steps 1–4 are the flyback converter specifications. The design equations for the transformer used in flyback converters for CCM operation are given in steps 5–14 [33]. Steps 15–19 are used in the calculation of area product. In steps 15 and 16, the values of window utilisation factor K_u and peak flux density B_{pk} are assumed to be 0.3 and 0.31 T, respectively. The typical values of K_u for transformers and inductors are 0.3 and 0.4, respectively. The typical range of values of saturation flux density B_s for ferrite core material at high temperatures is 0.3–0.35 T. In step 17, the value of current density J_m is assumed to be 6 A/mm^2. The typical range of J_m for power converter applications is 0.1–8 A/mm^2. Using the value of area product calculated in step 19 and using the manufacturer's datasheets, the parameters of the selected core are listed in steps 20–29. In order to mitigate the influence of skin effect, several strands of copper wires are used to make the primary and secondary winding wires. The diameter of the bare strand is taken to be twice the value of skin depth δ_w.

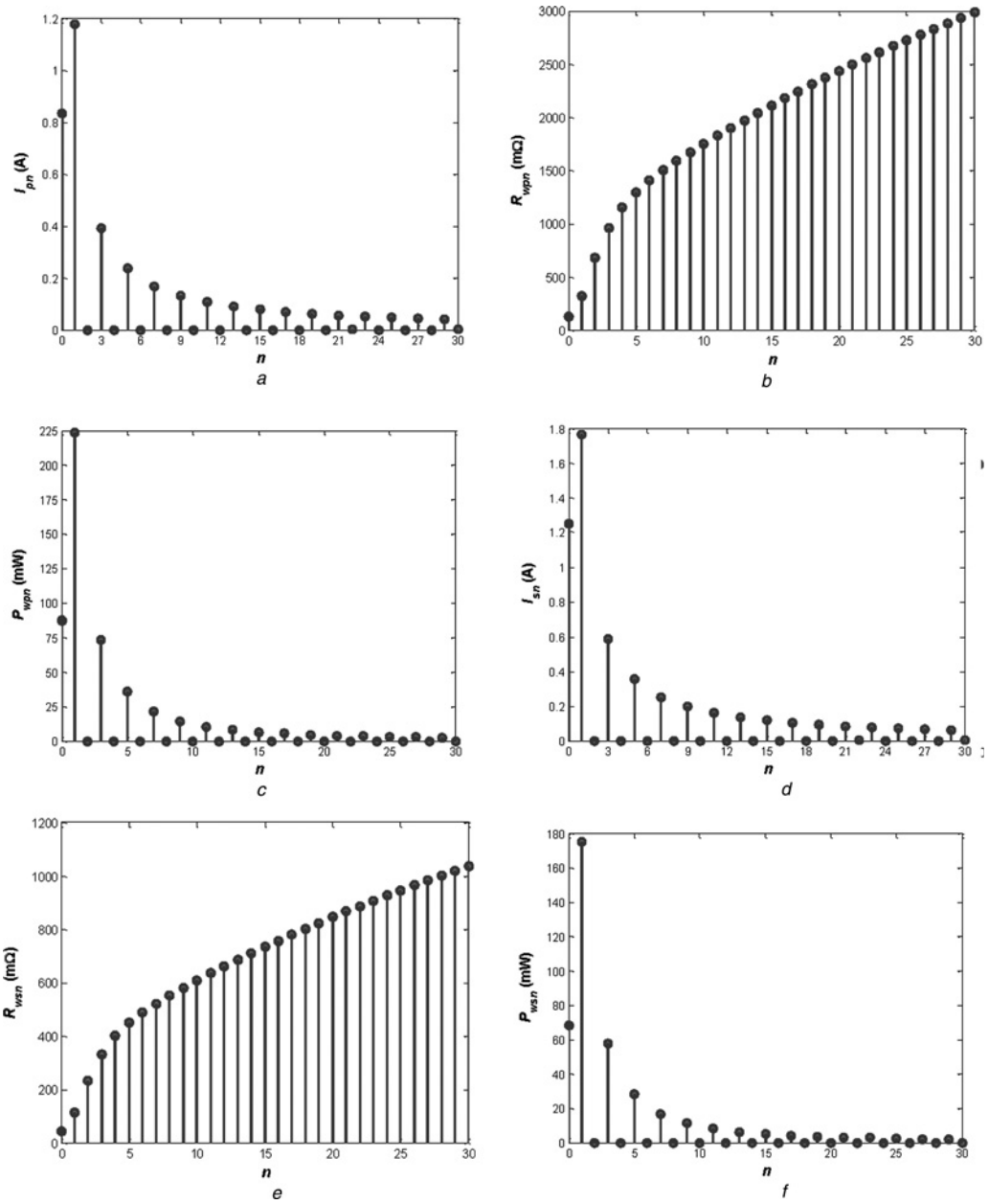

Fig. 5 *Spectra of primary and secondary currents, winding resistances and winding power losses*

a Amplitudes of the fundamental component and the harmonics of the flyback transformer primary winding current in CCM at minimum DC input voltage V_I and maximum output power P_O

b Spectrum of the primary winding AC resistance of the flyback transformer

c Spectrum of the primary winding power loss of the flyback transformer at minimum DC input voltage V_I and maximum output power P_O

d Amplitudes of the fundamental component and the harmonics of the flyback transformer secondary winding current in CCM at minimum DC input voltage V_I and maximum output power P_O

e Spectrum of the secondary winding AC resistance of the flyback transformer

f Spectrum of the secondary winding power loss of the flyback transformer at minimum DC input voltage V_I and maximum output power P_O

The value of skin depth δ_w which is a function of converter switching frequency f_s is calculated in step 30. The parameters of the selected strand wire are listed in steps 31–36. Equations in steps 37–40 and 46–50 are used to determine the number of turns and the number of strands of primary and secondary windings, respectively. Steps 41–45 and 51–55 are used to estimate the DC resistances and the power losses of primary and secondary windings, respectively. The total DC power loss and the total winding power loss are estimated using steps 56 and 57, respectively. Steps 58–62 are used to estimate the transformer core loss. In step 61, the core power loss density is estimated using the Steinmetz equation [40, 41]. Step 63 gives the total transformer power loss. Steps 64–66 are used to estimate the temperature rise of the transformer. In step 66, an empirical formula is used to estimate the rise in temperature of the transformer [30]. The assumption of the value of K_u in step 15 is rechecked in step 67. The efficiency of the transformer estimated at full power and minimum DC input voltage is given in step 68.

5 Characteristics of a HF transformer for flyback converters in CCM

In this section, the computed characteristics of the designed flyback transformer are presented for a wide range of

doi: 10.1049/iet-pel.2010.0040

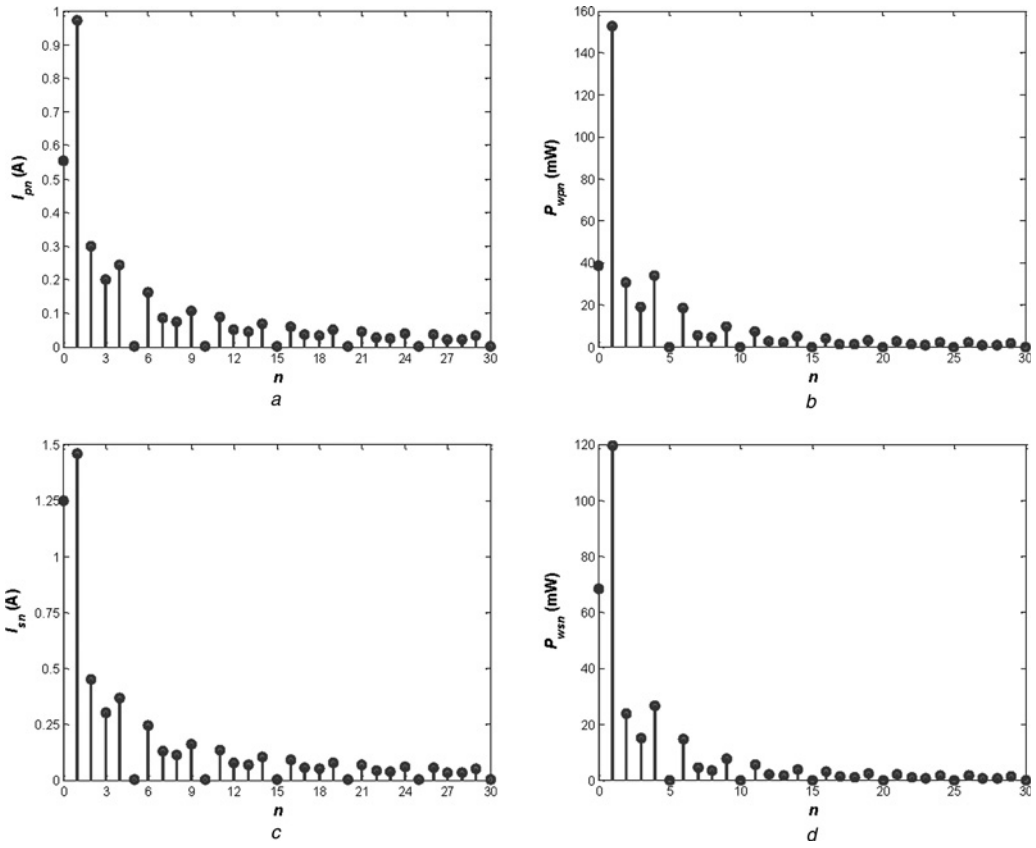

Fig. 6 *Spectra of primary and secondary currents and winding power losses*

a Amplitudes of the fundamental component and the harmonics of the flyback transformer primary winding current in CCM at maximum DC input voltage V_{I} and maximum output power P_{O}
b Spectrum of the primary winding power loss of the flyback transformer at maximum DC input voltage V_{I} and maximum output power P_{O}
c Amplitudes of the fundamental component and the harmonics of the flyback transformer secondary winding current in CCM at maximum DC input voltage V_{I} and maximum output power P_{O}
d Spectrum of the secondary winding power loss of the flyback transformer at maximum DC input voltage V_{I} and maximum output power P_{O}

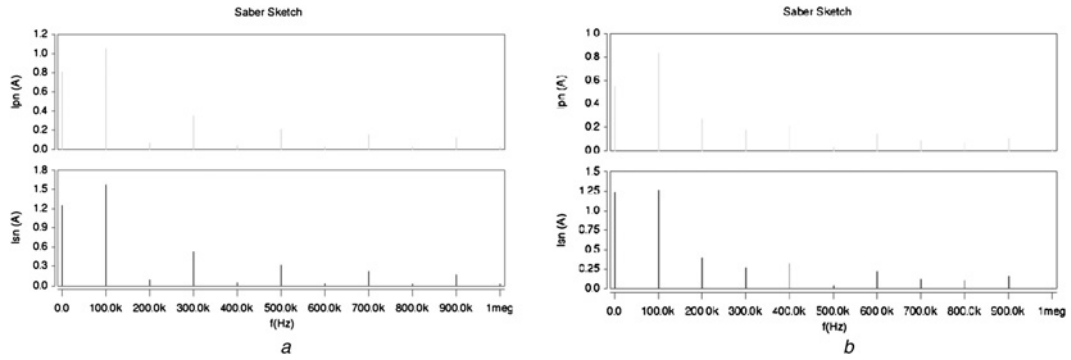

Fig. 7 *Simulation results of the amplitudes of the fundamental component and the harmonics of the flyback transformer winding currents in CCM*

a Converter operating at minimum DC input voltage V_{Imin} and maximum output power P_{Omax}. Top trace: I_{pn} for primary winding current waveform. Bottom trace: I_{sn} for secondary winding current waveform
b Converter operating at maximum DC input voltage V_{Imax} and maximum output power P_{Omax}. Top trace: I_{pn} for primary winding current waveform. Bottom trace: I_{sn} for secondary winding current waveform

operating conditions of the flyback converter in CCM, that is, over the entire range of the load current and the DC input voltage. Fig. 2 shows the primary winding harmonic loss factor F_{Rph} and the secondary winding harmonic loss factor F_{Rsh} as functions of input voltage V_{I} computed using (14), (15), (20), (26) and (27) at $N_l = 2$, $d/\delta_{w1} = 1.9378$, $d/p = 0.8$ and $n = 100$. It is clearly seen that the maximum value of F_{Rph} occurs at maximum input voltage. This is because at maximum input voltage, the duty cycle is low and the width of the primary winding current waveform is low and contains many significant harmonics. It is also seen that the maximum value of F_{Rsh} occurs at minimum input voltage. This is because at minimum input voltage, the duty cycle is high and the width of the secondary winding current is low and contains many significant harmonics. For CCM operation, F_{Rph} and F_{Rsh} are independent of the load current. The value of F_{Rph} and F_{Rsh} at the minimum input voltage for a specific case of the CCM flyback transformer

is predicted to be 5.195. Using F_{Rph} and the primary winding DC power loss obtained in step 45, primary winding loss P_{wp} as functions of input voltage and output power is plotted in Fig. 3*a*. The maximum primary winding power loss occurs at full load and minimum input voltage. Using F_{Rsh} and the secondary winding DC power loss obtained in step 55, secondary winding loss P_{ws} as functions of input voltage and output power is depicted in Fig. 3*b*. The maximum secondary winding power loss occurs at full load and minimum input voltage. The plot of total winding power loss P_w of the transformer as functions of input voltage and output power is shown in Fig. 3*c*. The maximum total winding power loss occurs at full load and minimum input voltage.

The variation of core loss P_C as a function of input voltage is shown in Fig. 4*a*. The core loss is calculated using steps 12, 29 and 58–62 in Table 1. The total power loss P_{cw} of the transformer as functions of input voltage and output power is shown in Fig. 4*b*. The maximum total power loss of the transformer occurs at full load and minimum input voltage. Fig. 4*c* shows the temperature rise ΔT in the flyback transformer as functions of input voltage and output power. The plot of transformer efficiency η_t as functions of input voltage and output power is shown in Fig. 4*d*. As expected, the minimum efficiency of the transformer occurs at full load and minimum input voltage.

Figs. 5*a*–*c* show the spectra of the primary winding current, the primary winding AC resistance and the primary winding power loss computed using (11), (14) and (13), respectively, for the flyback transformer in CCM at full load and minimum input voltage. Figs. 5*d*–*f* shows the spectra of the secondary winding current, the secondary winding AC resistance and the secondary winding power loss calculated using (24), (27) and (25), respectively, for the flyback transformer in CCM at full load and minimum input voltage. Figs. 6*a* and *b* show the spectra of the primary winding current and the primary winding power loss computed using (11) and (13), respectively, for the flyback transformer in CCM at full load and maximum input voltage. Figs. 6*c* and *d* show the spectra of the secondary winding current and the secondary winding power loss using (24) and (25), respectively, for the flyback transformer in CCM at full load and maximum input voltage. The winding resistance is independent of both the input voltage and the load current.

6 Experimental and simulation results

The designed transformer was built and the winding DC and AC resistances were measured at selected frequencies using Hewlett Packard 4275A multi-frequency LCR meter. The AC resistances of the primary winding of the transformer measured at 100, 200, and 400 kHz were 0.386, 0.861 and 1.588 Ω, respectively, and were in good agreement with the theoretical values presented in Fig. 5*b*. The AC resistances of the secondary winding of the transformer measured at 100, 200, and 400 kHz were 0.275, 0.706, and 1.404 Ω, respectively, and were in fairly good agreement with the theoretical values presented in Fig. 5*e*.

The parameters extracted from the constructed two-winding flyback transformer were used in the transformer for the simulation of a flyback converter in CCM. Figs. 7*a* and *b* show the spectra of the primary and secondary winding currents for minimum and maximum DC input voltages, respectively, for the flyback transformer in CCM at full load, obtained from Saber Sketch simulation. The theoretical values of the amplitudes of the fundamental component and the harmonics of the primary and secondary current waveforms of the flyback transformer predicted in Figs. 5 and 6 were in excellent agreement with the simulated waveforms of Fig. 7.

Measurement of the winding losses is a challenging problem, especially with the current harmonics present in the primary and the secondary windings. A major difficulty is to separate the winding losses and the core loss. Also, the other component losses have to be considered while measuring the converter efficiency. Therefore the theory proposed in this paper is validated by presenting the experimental results of the winding DC and AC resistances measured at the fundamental frequency and several harmonics for the windings of the constructed transformer along with simulation results depicting the spectra of currents in primary and secondary windings of the two-winding transformer used in a flyback converter.

7 Conclusions

Expressions for the primary and secondary winding power losses for periodic non-sinusoidal transformer current waveforms have been derived. A transformer has been designed for a flyback converter in CCM and its performance has been evaluated as functions of the output power and DC input voltage. The resistances of both windings have been measured at selected frequencies. It has been shown that the primary winding harmonic loss factor F_{Rph} increases as the DC input voltage V_I increases because the duty cycle decreases with increase in V_I. In contrast, the secondary winding harmonic loss factor F_{Rsh} decreases as the DC input voltage increases because the width of the secondary current increases with increase in V_I. Both these factors are independent of the output power. The winding power losses caused by the harmonics of the primary and secondary currents are not negligible for CCM operation of isolated PWM converters. This is because the spectra of the winding currents are very rich as opposed to the inductor current spectrum in non-isolated PWM converters. The maximum power loss in each winding occurs at the minimum DC input voltage V_I and the maximum output power P_O for the CCM flyback converter. A similar procedure to evaluate the winding power losses in transformers can be used for other isolated converters.

8 References

1 Tan, G.H., Wang, J.Z., Ji, Y.C.: 'Soft-switching flyback inverter with enhanced power decoupling for photovoltaic applications', *IET Proc. Electr. Power Appl.*, 2007, **1**, (2), pp. 264–274

2 Lai, C.M., Shyu, K.K.: 'A single-stage AC/DC converter based on zero voltage switching LLC resonant topology', *IET Proc. Electr. Power Appl.*, 2007, **1**, (5), pp. 743–752

3 Wai, R.J., Lin, C.Y., Liu, L.W., Chang, Y.R.: 'High efficiency single-stage bidirectional with multiple-input power sources', *IET Proc. Electr. Power Appl.*, 2007, **1**, (5), pp. 763–777

4 Lin, B.R., Huang, C.L., Li, M.Y.: 'Novel zero voltage switching dual-switch forward converter with ripple current cancellation', *IET Proc. Electr. Power Appl.*, 2007, **1**, (5), pp. 799–807

5 Lin, B.R., Huang, C.L.: 'Zero voltage switching active clamp buck-boost stage Ćuk converter', *IET Proc. Electr. Power Appl.*, 2007, **1**, (2), pp. 173–182

6 Bennett, E., Larson, S.C.: 'Effective resistance to alternating currents of multilayer windings', *Trans. AIEE*, 1940, **59**, pp. 1010–1016

7 Dowell, P.L.: 'Effect of eddy currents in transformer windings', *IEE Proc.*, 1966, **113**, (8), pp. 1387–1394

doi: 10.1049/iet-pel.2010.0040

8 Perry, M.P.: 'Multiple layer series connected winding design for minimum losses', *IEEE Trans. Power Appar. Syst.*, 1979, **98**, (1), pp. 116–123
9 Venkatraman, P.S.: 'Winding eddy current losses in switch mode power transformers due to rectangular wave currents'. Proc. POWERCON 11, Section A-1, 1984, pp. 1–11
10 Carsten, B.: 'High frequency conductor losses in switchmode magnetics'. Proc. HPFC, May 1986, pp. 155–176
11 Jongsma, J.: 'Minimum loss transformer windings for ultrasonic frequencies–part 2: transformer winding design'. Philips Electronics Application Bulletin E. A. B. vol. 35, pp. 211–226
12 Jongsma, J.: 'High-frequency ferrite power transformer and choke design–part 3: transformer winding design'. Philips Electron – Comp. and Materials Tech. vol. 207, pp. 1–28
13 Vandelac, J., Ziogas, P.D.: 'A novel approach for minimizing high-frequency transformer copper losses', *IEEE Trans. Power Electron.*, 1988, **3**, (3), pp. 166–176
14 Rosa, J.: 'Calculation of flux linkages in multiwinding transformers'. IEEE Power Electronics Specialists Conf. Record, 1986, 86CH2310-1, pp. 639–644
15 Coonrod, N.R.: 'Transformer computer design aid for higher frequency switching power supplies'. IEEE Power Electronics Specialists Conf. Record, 1984, 84CH2000-8, pp. 257–267
16 Hurley, W.G., Gath, E., Breslin, J.G.: 'Optimizing the AC resistance of multilayer transformer windings with arbitrary current waveforms', *IEEE Trans. Power Electron.*, 2000, **15**, (2), pp. 369–376
17 Urling, A.M., Niemela, V.A., Skutt, G.R., Wilson, T.G.: 'Characterizing high-frequency effects in transformer windings – a guide to several significant articles'. IEEE APEC, March 1989, pp. 373–385
18 Kassakian, J.G., Schlecht, M.F.: 'High-frequency high-density converters for distributed power-supply systems', *Proc. IEEE*, 1988, **76**, pp. 362–376
19 Williams, R., Grant, D.A., Gowar, J.: 'Multielement transformers for switched-mode power-supplies: toroidal designs', *IEE Proc., B*, 1993, **140**, (2), pp. 152–160
20 Cheng, K.W.E., Evans, P.D.: 'Calculation of winding losses in high-frequency toroidal inductors using multistrand conductors', *IEE Proc., B, Electric Power Appl.*, 1995, **142**, (5), pp. 313–322
21 Cheng, K.W.E., Evans, P.D.: 'Calculation of winding losses in high-frequency toroidal inductors using single strand conductors', *IEE Proc. B, Electric Power Appl.*, 1994, **141**, (2), pp. 52–62
22 Evans, P.D., Chew, W.M.: 'Reduction of proximity losses in coupled inductors', *Proc. Inst. Elect. Eng. B*, 1991, **138**, (2), pp. 51–58
23 Hanselman, D.C., Peake, W.H.: 'Eddy-current effects in slot-bound conductors', *Proc. Inst. Elect. Eng. B, Electr. Power Appl.*, 1995, **142**, pp. 131–136
24 Hurley, W.G., Wölfle, W., Breslin, J.G.: 'Optimized transformer design: inclusive of high frequency effects', *IEEE Trans. Power Electron.*, 1998, **13**, (4), pp. 651–659
25 Petkov, R.: 'Optimized design of a high-power high-frequency transformer', *IEEE Trans. Power Electron.*, 1996, **11**, (1), pp. 33–42
26 Bartoli, M., Reatti, A., Kazimierczuk, M.K.: 'Modeling iron-powder inductors at high-frequencies'. IEEE Proc. Industry Applications Society Annual Meeting, Denver, USA, October 1994, pp. 1225–1232
27 Bartoli, M., Noferi, N., Reatti, A., Kazimierczuk, M.K.: 'Modeling winding losses in high-frequency power inductors', *J. Circuits, Syst. Comput.*, 1995, **5**, (4), pp. 607–626
28 Bartoli, M., Noferi, N., Reatti, A., Kazimierczuk, M.K.: 'Modeling litz-wire winding losses in high-frequency power inductors'. IEEE Power Electronics Specialists Conf. Record, 1996, pp. 1690–1696
29 Grandi, G., Kazimierzcuk, M.K., Massarini, A., Reggiani, U., Sancineto, G.: 'Model of laminated iron-core inductors', *IEEE Trans. Magn.*, 2004, **40**, (4), pp. 1839–1845
30 McLyman, W.T.: 'Transformer and inductor design handbook' (Marcel Dekker, 2004, 3rd edn.)
31 Kazimierczuk, M.K., Sekiya, H.: 'Design of AC resonant inductors using area product method'. Proc. IEEE First Energy Conversion Conf., 2009, pp. 994–1001
32 Sekiya, H., Kazimierczuk, M.K.: 'Design of RF-choke inductors using core geometry coefficient'. Proc. Electrical Manufacturing and Coil Winding Conf., 2009
33 Kazimierczuk, M.K.: 'Pulse-width modulated DC–DC power converters' (John Wiley & Sons, 2008)
34 Murthy-Bellur, D., Kazimierczuk, M.K.: 'Two-switch flyback PWM DC–DC converter in discontinuous-conduction mode', *Int. J. Circuit Theory Appl.*, (To be published), Early view published online: April 2010, DOI: 10.1002/cta.672, http://onlinelibrary.wiley.com/doi/10.1002/cta.672/pdf
35 Murthy-Bellur, D., Kazimierczuk, M.K.: 'Two-switch flyback PWM DC–DC converter in continuous-conduction mode', *Int. J. Circuit Theory Appl.*, (To be published), Early view published online: July 2010, DOI: 10.1002/cta.690, http://onlinelibrary.wiley.com/doi/10.1002/cta.690/pdf
36 Murthy-Bellur, D., Kazimierczuk, M.K.: 'Harmonic winding loss in buck DC–DC converter for discontinuous conduction mode', *IET Power Electron.*, 2010, **3**, (5), pp. 740–754
37 Murthy-Bellur, D., Kazimierczuk, M.K.: 'Winding losses caused by harmonics in high-frequency flyback transformers for pulse-width modulated dc–dc converters in discontinuous conduction mode', *IET Power Electron.*, 2010, **3**, (5), pp. 804–817
38 Kondrath, N., Kazimierczuk, M.K.: 'Inductor winding loss owing to skin and proximity effects including harmonics in non-isolated pulse-width modulated dc–dc converters operating in continuous conduction mode', *IET Power Electron.*, 2010, **3**, (6), pp. 989–1000
39 Kazimierczuk, M.K.: 'High-frequency magnetic components' (John Wiley & Sons, 2009)
40 Steinmetz, C.P.: 'On the law of hysteresis', *AIEE Trans.*, 1892, **9**, pp. 3–64
41 Magnetics incorporated: 'Curve fit equations for ferrite material'. Technical Bulletin FC-S7, available at http://www.mag-inc.com/design/technical-documents, accessed July 2009, pp. 1–6